1184 *Biochemistry* **2011,** *50,* 1184–1193
DOI: 10.1021/bi101721f

BIOCHEMISTRY
including biophysical chemistry & molecular biology
*Article*

# Phosphoenolpyruvate: Sugar Phosphotransferase System from the Hyperthermophilic *Thermoanaerobacter tengcongensis*[†]

Vera Navdaeva, Andreas Zurbriggen, Sandro Waltersperger, Philipp Schneider, Anselm E. Oberholzer, Priska Bähler, Christoph Bächler, Andreas Grieder, Ulrich Baumann,* and Bernhard Erni*

*Departement für Chemie und Biochemie (or Department for Chemistry and Biochemistry), Universität Bern, Freiestrasse 3, CH-3012 Bern, Switzerland*

*Received October 26, 2010; Revised Manuscript Received December 23, 2010*

ABSTRACT: *Thermoanaerobacter tengcongensis* is a thermophilic eubacterium that has a phosphoenolpyruvate (PEP) sugar phosphotransferase system (PTS) of 22 proteins. The general PTS proteins, enzyme I and HPr, and the transporters for *N*-acetylglucosamine (EIICB$^{GlcNAc}$) and fructose (EIIBC$^{Fru}$) have thermal unfolding transitions at ~90 °C and a temperature optimum for in vitro sugar phosphotransferase activity of 65 °C. The phosphocysteine of a EIICB$^{GlcNAc}$ mutant is unusually stable at room temperature with a $t_{1/2}$ of 60 h. The PEP binding C-terminal domain of enzyme I (EIC) forms a metastable covalent adduct with PEP at 65 °C. Crystallization of this adduct afforded the 1.68 Å resolution structure of EIC with a molecule of pyruvate in the active site. We also report the 1.83 Å crystal structure of the EIC−PEP complex. The comparison of the two structures with the apo form and with full-length EI shows differences between the active site side chain conformations of the PEP and pyruvate states but not between the pyruvate and apo states. In the presence of PEP, Arg465 forms a salt bridge with the phosphate moiety while Glu504 forms salt bridges with Arg186 and Arg195 of the N-terminal domain of enzyme I (EIN), which stabilizes a conformation appropriate for the in-line transfer of the phosphoryl moiety from PEP to His191. After transfer, Arg465 swings 4.8 Å away to form an alternative salt bridge with the carboxylate of Glu504. Glu504 loses the grip of Arg186 and Arg195, and the EIN domain can swing away to hand on the phosphoryl group to the phosphoryl carrier protein HPr.

The phosphoenolpyruvate (PEP):sugar phosphotransferase system (PTS)[1] mediates carbohydrate uptake by a mechanism that couples translocation of the substrate with its phosphorylation (group translocation) (*1*). PEP is the phosphoryl donor, and phosphoryl groups are transferred by a chain of four phosphoproteins that are transiently phosphorylated at histidine or cysteine residues (Figure 1). The first component of this chain is enzyme I (EI, PtsI, or PtsA), a two-domain protein that is autophosphorylated by PEP. The phosphate is then transferred to the histidine-containing phosphoryl carrier protein HPr (PtsH). This small 9 kDa protein distributes phosphoryl groups to the sugar-specific transporters (enzymes II$^{sugar}$ and EII). Each EII consists of three domains or subunits termed EIIA, EIIB, and EIIC. EIIA and EIIB are soluble, and EIIC is a multispanning membrane protein. EIIA mediates the transfer of phosphate from HPr to the EIIB unit, which then transfers the phosphate to the sugar transported by EIIC. EIIC itself is not phosphorylated. In addition to carbohydrate transport and phosphorylation, PTS proteins also play a central role in the control of the carbon and nitrogen metabolism. Depending on the organism and on the particular transporter, HPr, EIIA, and/or EIIB subunits regulate the activity of enzymes and transcription factors, allosterically or by reversible phosphorylation (for a review, see ref *2*). Control activity varies with the concentration ratio of the dephosphorylated (X) and the phosphorylated form (P-X) of these proteins. The X/P-X ratio reflects the availability of PTS substrates. The X/P-X ratio increases when a particular PTS sugar is actively transported, or when the PEP concentration decreases. The X/P-X ratio decreases in the absence of transportable substrates, when the phosphorylated form of the sugar-specific PTS proteins (P-EIIA and P-EIIB) accumulates (*3*, *4*). EI and HPr with a few exceptions are encoded only once per genome. PTS transporters, in contrast, are diverse with respect to both fold and sugar specificity. They can be grouped into five families of different and unrelated structures. PTS proteins have been detected in ~60% of the eubacteria (genomes) (*5*, *6*), in a few archaebacteria (*7*), but not in eukaryotes.

Structures for most of the cytoplasmic PTS subunits and domains have been determined by X-ray crystallography and NMR (for a review, see ref *8*). Of the membrane-spanning EIIC domains, however, only topology models exist (*9*−*14*).

Proteins of thermophilic bacteria are more rigid at low temperatures and therefore more suitable for crystallization. However, the

[†]This research was supported by Swiss National Science Foundation Grants 3100A0-105247 and A3100-120174.

*To whom correspondence should be addressed. B.E.: Departement für Chemie und Biochemie (or Department for Chemistry and Biochemistry), Universität Bern, Freiestrasse 3, CH-3012 Bern, Switzerland; telephone, ++41-31-6314346; fax, ++41-31-6314887; e-mail, bernhard.erni@ibc.unibe.ch. U.B.: Departement für Chemie, Universität Köln, Zülpicher Strasse 47, D-50674 Köln, Germany; telephone, 49-221-470-77867; e-mail, ulrich.baumann@uni-koeln.de.

[1]Abbreviations: PEP, phosphoenolpyruvate; PTS, PEP-dependent carbohydrate:phosphotransferase system; Prv, pyruvate; GlcNAc, *N*-acetylglucosamine; Glc, glucose; Fru, fructose; EI, enzyme I of the PTS; EIN and EIC, N- and C-terminal domains of EI, respectively; HPr, phosphoryl carrier protein of the PTS; EIICB$^{sugar}$, sugar-specific enzyme II of the PTS; *Tt*, *Thermoanaerobacter tengcongensis*; *Ec*, *Escherichia coli*; *Sa*, *Staphylococcus aureus*; MR, molecular replacement; CD, circular dichroism; DDM, *N*-dodecyl β-D-maltopyranoside; PMSF, phenylmethanesulfonyl fluoride; DTT, dithiothreitol; NTA, nitrilotriacetic acid; SDS−PAGE, polyacrylamide gel electrophoresis in the presence of sodium dodecyl sulfate; rmsd, root-mean-square deviation.

 Published on Web 01/02/2011 

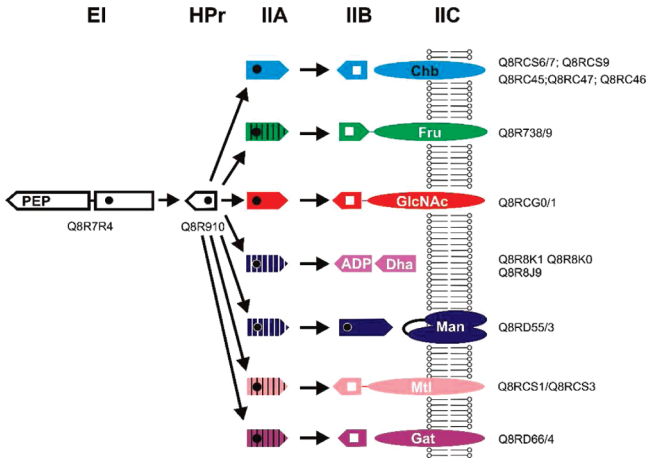


FIGURE 1: PTS of *Thermoanaerobacter tengcongensis*. Functional units EI, HPr, EIIA, EIIB, and EIIC are vertically aligned. Circles and squares denote phosphorylated His and Cys residues, respectively. Pointed ends indicate the carboxy-terminal end of the polypeptide chain of the subunits and of the cytoplasmic domains within multidomain proteins. The two subunits of the dihydroxyacetone (Dha) kinase (purple) are soluble. The subunit analogous to EIIB contains ADP as a cofactor (*40*, *41*). Thin arrows denote the physiological direction of the phosphoryl transfer reactions. SWISS-PROT accession codes of the PTS transporter subunits are given at the right. The predicted substrate specificities are as follows: Chb, chitobiose; Fru, fructose, GlcNAc, *N*-acetylglucosamine; Dha, dihydroxyacetone; Man, mannose; Mtl, mannitol; Gat, galacitol. Two paralogues of putative chitobiose transporters exist (Q8RC45–Q8RC47, Q8RCS6, Q8RCS7, and Q8RCS9).

two favorite thermophilic bacteria, *Thermotoga maritima* and *Aquifex aeolicus*, that optimally grow at 80−85 °C do not have a PTS. *Thermoanaerobacter tengcongensis* is a near-extreme thermophilic Gram-negative bacterium with a complete PTS. It grows optimally at 75 °C and pH 7.0−7.5 and metabolizes glucose, galactose, maltose, cellobiose, mannose, fructose, lactose, mannitol, and starch to mainly acetate and ethanol. The *T. tengcongensis* genome (*15*) contains genes for 22 PTS proteins (Figure 1): the general phosphoryl carrier proteins EI and HPr, a PTS-dependent dihydroxyacetone kinase, seven transporters (EIIA, EIIB, and EIIC subunits and/or domains) with proposed specificity for *N*-acetylglucosamine, fructose, mannose, cellobiose (two systems), mannitol, and galacitol. They display a high degree of sequence similarity with homologues from *Escherichia coli* and *Staphylococcus aureus*, for instance: EI (54% with *E. coli*, 53% with *S. aureus*), HPr (41%, 52%), $IIA^{GlcNAc}$ (47%, 53%), $EIICB^{GlcNAc}$ (54%, 53%), $EIIA^{Fru}$ (29%, 37%), and $EIIBC^{Fru}$ (55%, 50%). In view of this strong sequence similarity, *T. tengcongensis* may be a useful source for structural studies of proteins that have been functionally characterized in *E. coli* but could not yet be crystallized. Here, we have purified and characterized in vitro the PTS for GlcNAc and for Fru of *T. tengcongensis*. In the course of this study, we also determined the structures of the EIC−PEP enzyme substrate and the EIC−pyruvate product complexes.

## EXPERIMENTAL PROCEDURES

*Bacterial Strains, Plasmids, and Media*. *E. coli* strain ZSC112LΔLPMΔnagE (*ptsG*, *manXYZ*, *nagE*, *glk*) was used for protein expression and in vivo complementation with EI and $EIICB^{GlcNAc}$, respectively. Strain ZSC112LΔHIC (*ptsHIcrr*, *ptsG*, *manZ*, *glk*) was used for the expression of nonphosphorylated $EIICB^{GlcNAc}$. Genomic DNA of *T. tengcongensis* MB4T (DSMZ15242) was used as template for PCR amplification of PTS genes.

The *ptsA* (EI, Q8R7R4), *fruB* (HPr, Q8R910), *nagE* ($IIA^{GlcNAc}$, Q8RCG0), and *ptsG* ($EIICB^{GlcNAc}$, Q8RCG1 corrected for 14 upstream codons) coding sequences were PCR amplified with 5′ primers encoding TG (NdeI, half-site) and 3′ primers encoding a *Bam*HI (or *Bgl*II or *Eco*RI) restriction site and cloned in expression plasmids pJF119EH (modified to encode a C-terminal histidine tag) or pET28a(+). Point mutations were introduced by QuikChange (Stratagene) mutagenesis. The sequences of the oligonucleotide primers are listed in Table S1 of the Supporting Information, and experimental details are also given as Supporting Information.

*Expression and Purification of T. tengcongensis PTS Proteins*. *E. coli* were grown in Erlenmeyer flasks on an orbital shaker at 37 °C until $A_{550}$ reached 1.3, and protein expression was induced with 0.2 mM isopropyl β-D-thiogalactopyranoside (IPTG). After being induced for 4 h, cells were harvested by centrifugation and lysed in a French pressure cell (1000 psi). Cytoplasmic and membrane fractions were separated by high-speed centrifugation. EI, HPr, and IIAs (all with N-terminal histidine tags) were purified by $Ni^{2+}$-NTA chromatography and gel filtration chromatography.

$EIICB^{GlcNAc}$ with N- or C-terminal and $EIIBC^{Fru}$ with N-terminal histidine tags were purified and solubilized with *N*-dodecyl β-D-maltopyranoside (DDM, Anatrace) and purified by $Ni^{2+}$-NTA and gel filtration chromatography in the presence of 0.4 mM DDM. The details are given in the Supporting Information.

*Thermal Unfolding and Circular Dichroism (CD) Spectroscopy*. The progress of temperature-induced unfolding was monitored at 222 nm in a 0.1 cm cuvette using a Jasco J-715 spectropolarimeter (Jasco, Tokyo, Japan) equipped with a Peltier temperature controller (PFD-3505, Jasco, 1 °C/min from 30 to 100 °C). The midpoint of the thermal unfolding transition ($T_m$) was calculated as the maximal value of the first derivative of the CD signal at 222 nm with respect to temperature. Protein concentrations were between 0.3 and 0.5 mg/mL (or as indicated). The details are given in the Supporting Information.

*PEP-Sugar Phosphotransferase Assay*. The phosphotransferase activity of the *T. tengcongensis* PTS at 65 °C and of the *E. coli* PTS at 37 °C was assayed by the ion exchange method of Kundig and Roseman (*16*, *17*), in the presence of saturating concentrations of EI, HPr, and $EIIA^{sugar}$. The details are given in the Supporting Information.

*Assay for Protein Phosphorylation and Dephosphorylation*. Phosphorylation of all PTS proteins was assayed by incubation with [$^{32}$P]PEP, gel electrophoretic separation of the proteins, and autoradiography followed by protein staining of the gels. Phosphorylation of $EIICB^{GlcNAc}$ could also be detected by the electrophoretic mobility shift. The samples were incubated for 10 min at 65 °C. The details are given in the Supporting Information.

*Crystallization and Structure Determination*. Orthorhombic crystals of EIC with PEP were obtained within 12 h by vapor diffusion in 2 μL sitting drops [1 μL of EIC (12 mg/mL) and 1 μL of reservoir buffer] over 70 μL of reservoir buffer [5 mM PEP, 0.1 M succinic acid (pH 7.0), and 15% PEG3350] at 20 °C. Crystals were cryoprotected by increasing the PEG3350 concentration of the crystallization buffer to 37.5% and flash-cooled in liquid nitrogen. The crystals belong to orthorhombic space group

Table 1: Data Collection and Refinement Statistics for EIC−PEP and EIC−Prv Complexes

| | EIC−PEP | EIC−pyruvate |
|---|---|---|
| space group | $P2_12_12$ | $P2_12_12_1$ |
| *a*, *b*, *c* (Å) | 83.50, 92.13, 47.07 | 60.12, 79.53, 156.75 |
| α, *β*, *γ* (deg) | 90, 90, 90 | 90, 90, 90 |
| no. of molecules per asymmetric unit | 1 | 2 |
| Data Collection (XDS) | | |
| beamline | X06DA | X06DA |
| wavelength (Å) | 1.000 | 1.00 |
| resolution range (Å) | 100−1.83 | 100−1.68 |
| no. of observations | 103530 | 316596 |
| no. of unique reflections | 58115 | 86331 |
| completeness (%) | 93.6 (87.1)[a] | 99.4 (98.2)[a] |
| $R_{merge}$ (%)[b] | 5.4 (37.6)[a] | 3.8 (63.9)[a] |
| $I/\sigma I^2$ | 9.17 (2.05)[a] | 19.53 (2.00)[a] |
| Refinement (Phenix) | | |
| resolution range (Å) | 61.87−1.83 | 39.19−1.68 |
| no. of reflections in the working set | 55176 | 86329 |
| no. of reflections in the test set | 2891 | 2590 |
| $R/R_{free}$ (%) | 16.63/19.46 | 17.00/19.16 |
| no. of atoms | | |
| protein | 2588 | 5022 |
| ligand(s) | 11 | 14 |
| water | 371 | 648 |
| rmsd | | |
| bond lengths (Å) | 0.003 | 0.006 |
| bond angles (deg) | 0.762 | 0.968 |
| Ramachandran plot (%) | | |
| most favored | 98.5 | 98.3 |
| allowed | 1.5 | 1.7 |
| disallowed | 0 | 0 |
| mean *B* factor (Å$^2$) | | |
| main chain | 22.5 | 28.6 |
| side chain and waters | 31.4 | 36.4 |

[a]The values in parentheses correspond to those of the outermost resolution shell. [b]$R_{merge} = \sum_{hkl}\sum_j|I(hkl;j) - \langle I(hkl)\rangle|/[\sum_{hkl}\sum_j\langle I(hkl)\rangle]$, where $I(hkl;j)$ is the *j*th measurement of the intensity of unique reflection *hkl* and $\langle I(hkl)\rangle$ is the mean over all symmetry-related measurements.

$P2_12_12_1$ with one EIC monomer per asymmetric unit and the following cell parameters: $a$ = 83.50 Å, $b$ = 92.13 Å, $c$ = 47.07 Å. Diffraction data to 1.83 Å resolution were collected at beamline X06DA at the Swiss Light Source (Paul Scherrer Institute, Villigen, Switzerland).

Crystals of EIC with Prv were obtained as follows. The PEP concentration of the protein solution was increased to 5 mM, and the protein sample was incubated at 65 °C for 10 min prior to crystallization. Orthorhombic crystals of the EIC−Prv complex were observed after 3 weeks by the same procedure described above but with a different crystallization buffer [0.2 M KCl, 0.01 M $CaCl_2$, 0.05 M sodium cacodylate trihydrate (pH 6.0), and 10% PEG4000]. The crystals were dehydrated and cryoproteced via addition of sucrose to the crystal drop. The crystals belong to space group $P2_12_12_1$ with one biological EIC dimer per asymmetric unit and the following cell parameters: $a$ = 60.12 Å, $b$ = 79.53 Å, and $c$ = 156.75 Å. Diffraction data to 1.79 Å resolution were collected at beamline X06DA at the Swiss Light Source (Paul Scherrer Institute). The details of data processing and structure solution and the data collection and refinement statistics are listed in Table 1 and in the Supporting Information. The figures of the structural models were prepared with PYMOL (http://www.pymol.org). The coordinates and structure factors were deposited in the RCSB Protein Data Bank as entries 2XZ7 and 2XZ9.

## RESULTS AND DISCUSSION

*Protein Expression and Purification*. The *T. tengcongensis* proteins were expressed in *E. coli* K-12 and purified by $Ni^{2+}$-NTA affinity chromatography and gel filtration. EI with a C-terminal histidine tag initially was contaminated with several EI fragments. They all started at methionines, pointing to initiation of translation after rare codons. Production of these fragments could be strongly suppressed by (i) mutation of the four codons TTG62, GTG114, ATG115, and GTG250 (resulting in the two nonsilent changes M115L and V250L), (ii) moving the histidine tag from the C- to the N-terminus, and (iii) protein expression in *E. coli* Rosetta (DE3). Of all the other *T. tengcongensis* proteins, only the full-length forms were obtained (most likely because the truncated forms are not stable). The yields per liter of cell culture were 40 mg of EI and HPr and 10 mg of $EIIA^{GlcNAc}$. All proteins were more than 95% pure (Figure 2).

$EIICB^{GlcNAc}$ with either an N-terminal or C-terminal hexahistidine tag was solubilized with 60 mM DDM and purified by $Ni^{2+}$-NTA affinity chromatography. Notice that the true start codon of *ptsG* is located 42 bp upstream of the open reading frame indicated by the electronic annotation (Swiss-Prot entry Q8RCG1, TTE0468). Purified $EIICB^{GlcNAc}$ elutes upon gel filtration as an almost symmetrical peak at the elution volume corresponding to a 150 kDa globular protein (not shown). The protein yield after gel filtration was 1.5−2.5 mg/L of cell culture;

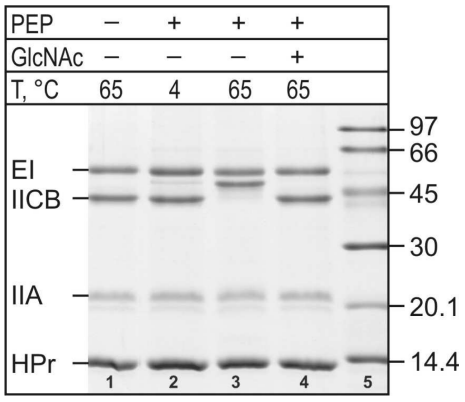


FIGURE 2: Polyacrylamide gel of purified *T. tengcongensis* PTS proteins and mobility shift of EIICB$^{GlcNAc}$ after phosphorylation. The mobility of EIICB$^{GlcNAc}$ is shifted only in the presence of PEP (compare lanes 1 and 3) and at 65 °C (compare lanes 2 and 3). EIICB$^{GlcNAc}$ is dephosphorylated in the presence of GlcNAc in excess over PEP (lane 4). For details, see Experimental Procedures. The proteins in the SDS sample buffer were not boiled before electrophoresis. The gel was stained with Coomassie blue.

70−90% of the phosphotransferase activity present in membranes was recovered, and the protein was more than 95% pure as judged by SDS−PAGE (Figure 2). No difference was observed between EIICB$^{GlcNAc}$ with N- and C-terminal histidine tags.

$Ni^{2+}$-NTA affinity chromatography afforded two EIICB$^{GlcNAc}$ species with apparent molecular mass of 45 and 50 kDa (SDS−PAGE). Both had identical N-terminal sequences and intact C-terminal histidine tags as determined by Edman sequencing and Western blotting with an anti-histidine antibody. The 50 kDa band disappeared upon incubation at 70 °C with 2 mM GlcNAc, and the amount of the 45 kDa species increased, suggesting that the former is the phosphorylated form of EIICB$^{GlcNAc}$. Only a single 45 kDa band was visible when EIICB$^{GlcNAc}$ was expressed in *E. coli* ZSC112LΔHIC that lacks the phosphotransferase proteins EI, HPr, and EIIA$^{Glc}$ (results not shown). That the electrophoretic mobility shift of EIICB$^{GlcNAc}$ is caused by phosphorylation was confirmed with purified PTS proteins in vitro. The upshift was observed only when EIICB$^{GlcNAc}$ was incubated with EI, HPr, EIIA$^{GlcNAc}$, and PEP (in the absence of GlcNAc) at 60 °C (Figure 2) but not at 4 °C. The 45 kDa band accumulates in the absence of PEP, or when EIICB$^{GlcNAc}$ was dephosphorylated with an excess of GlcNAc. A similar reduction in electrophoretic mobility is observed with phosphorylated *E. coli* EIIA$^{Glc}$ (*18*) possibly because the level of SDS binding is reduced by electrostatic repulsion between sulfate and phosphate/carboxylate.

The two subunits of the fructose transporter, EIIBC$^{Fru}$ and EIIA$^{Fru}$, with C-terminal histidine tags were purified by $Ni^{2+}$-NTA affinity chromatography. EIIA$^{Fru}$ was pure as judged by SDS−PAGE. The EIIBC$^{Fru}$ fraction contained a major band with an apparent molecular mass of 43 kDa and one faster-moving band. Both were excised and digested in gel with trypsin, and the tryptic fragments were analyzed by mass spectrometry (MALDI-TOF). The major band could thus be identified as full-length EIIBC$^{Fru}$ with intact N- and C-terminal ends. The shorter fragment starts with an intact N-terminus but ends shortly after residue 407. This region is highly variable in the alignment of nonredundant EIIBC$^{Fru}$ sequences and predicted to be exposed on the cytoplasmic side of the membrane (*19*, *20*). It is noteworthy that the truncated subunit has lost the histidine affinity tag. Retention of this fragment on the $Ni^{2+}$-NTA column suggests that it is copurified in a heterodimer with full-length EIIBC$^{Fru}$ (results not shown).

Attempts to overexpress the other PTS transporters in *E. coli* failed for various reasons. Of the mannose transporter consisting of an EIIA$^{Man}$ subunit, an EIIB$^{Man}$ subunit, and a two-domain membrane-spanning EIICD$^{Man}$ subunit (rather than an EIIC$^{Man}$ subunit and an EIID$^{Man}$ subunit as in *E. coli*), only EIIA$^{Man}$ and EIIB$^{Man}$ were expressed. EIICD$^{Man}$ could not be detected either as a Coomassie blue-stained protein band or with an anti-histidine antibody. The putative transporter for chitobiose, EIIC$^{Chb}$, also could not be expressed in *E. coli*. The putative galacitol transporter, IIC$^{Gat}$, could be expressed; however, protein yields were frustratingly small, and purification was inefficient compared to that of EIIBC$^{Fru}$ and EIICB$^{GlcNAc}$ (*21*). Expression of the mannitol transporter appears to be highly toxic, because no transformants encoding an intact *mtlA* gene could be isolated. The first two-thirds and the last two-thirds of the *mtlA* gene could be cloned separately, but the full-length *mtlA* gene could not be assembled from these parts. The few transformants that grew formed small colonies and contained plasmids with deletions and/or inversions within the *mtlA* gene (*22*).

*Sugar Phosphotransferase Activity of the Purified T. tengcongensis Protein*. The temperature optimum of the *T. tengcongensis* PTS was determined with purified EI, HPr, EIIA$^{GlcNAc}$, and either washed *E. coli* membranes containing EIICB$^{GlcNAc}$ or purified EIICB$^{GlcNAc}$. The temperature optimum of the *T. tengcongensis* GlcNAc PTS is 65 °C. At 50 and 75 °C, the activity was reduced to 50%, and at 30 and 90 °C, the system is not active (Figure 3A). None of *T. tengcongensis* proteins complemented sugar phosphotransferase activity in *E. coli* at 37 °C as indicated by the yellow color of the colonies on McConkey sugar indicator plates (results not shown). The sugar binding and membrane-spanning EIIC domain of EIICB$^{GlcNAc}$ of *T. tengcongensis* shares 60 and 45% sequence identity with the EIIC domains of *E. coli* EIICBA$^{GlcNAc}$ and EIICB$^{Glc}$, respectively. The phosphotransferase specificity of *T. tengcongensis* EIICB$^{GlcNAc}$ was characterized with [$^{14}$C]GlcNAc and [$^{14}$C]Glc in vitro. GlcNAc is a better substrate than Glc, but the latter is also phosphorylated with a $V_{max}$ of 25% relative to GlcNAc, confirming the prediction that EIICB$^{GlcNAc}$ is an GlcNAc-specific transporter (*23*). EIICB$^{Glc}$ of *E. coli*, for comparison, is more specific for Glc and has almost no activity for GlcNAc (Figure 3B). Purified EIIBC$^{Fru}$ and EIIA$^{Fru}$ are also active under similar conditions but 30−10 times less active than EIICB$^{GlcNAc}$ (Figure 3C).

*Stability of T. tengcongensis Proteins against Heat-Induced Denaturation*. The *T. tengcongensis* PTS proteins share more than 50% sequence identity with the homologous proteins of *E. coli* and *Bacillus subtilis*; however, *T. tengcongensis* optimally grows at 75 °C, whereas the mesophilic bacteria have growth optima below 40 °C. The stabilities of the *T. tengcongensis* proteins were determined by heat-induced unfolding. The transition temperatures ($T_m$) were determined from the first derivatives of the unfolding curves monitored by CD spectroscopy (Figures S1 and S2 of the Supporting Information).

Unfolding of HPr and and unfolding of EIICB$^{GlcNAc}$ are "two-state" transitions (Figure S1A,C of the Supporting Information). The $T_m$ of HPr is 84 °C, and that of EIICB$^{GlcNAc}$ is 85 °C. Both proteins are completely unfolded at 90 °C, consistent with the observed inactivation of in vitro phosphotransferase activity at this temperature (Figure 3A). The ellipticity of $\beta$-sheet protein EIIA$^{Glc}$ first increases at 84 °C and then decreases

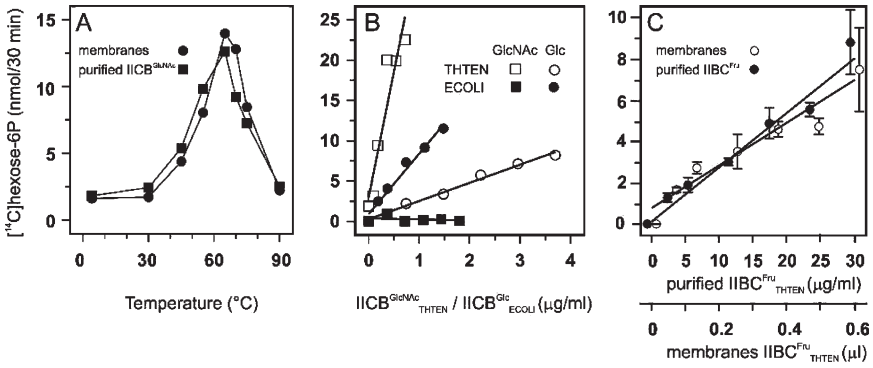


FIGURE 3: Sugar phosphotransferase activity of PTS proteins. (A) Temperature optima of purified EIICB$^{GlcNAc}$ and of an EIICB$^{GlcNAc}$-containing membrane preparation of *E. coli*. (B) Comparison of substrate specificities and activities of the GlcNAc PTS of *T. tengcongensis* and of the homologous Glc PTS of *E. coli*. *E. coli* EIICB$^{Glc}$ is Glc-specific, and *T. tengcongensis* EIICB$^{GlcNAc}$ has a relaxed specificity for both substrates. EIICBs were titrated in the presence of saturating concentrations of soluble PTS proteins as well as of [$^{14}$C]GlcNAc or [$^{14}$C]Glc ($V_{max}$ conditions). (C) Fructose PTS activity of purified EIIBC$^{Fru}$ and of an EIIBC$^{Fru}$-containing membrane preparation. EIICB$^{GlcNAc}$ and EIIBC$^{Fru}$ activities were assayed in the presence of EI, HPr, and EIIA$^{GlcNAc}$ or EIIA$^{Fru}$ of *T. tengcongensis* at 65 °C (A−C) and the corresponding *E. coli* proteins at 37 °C (B). For details, see Experimental Procedures.

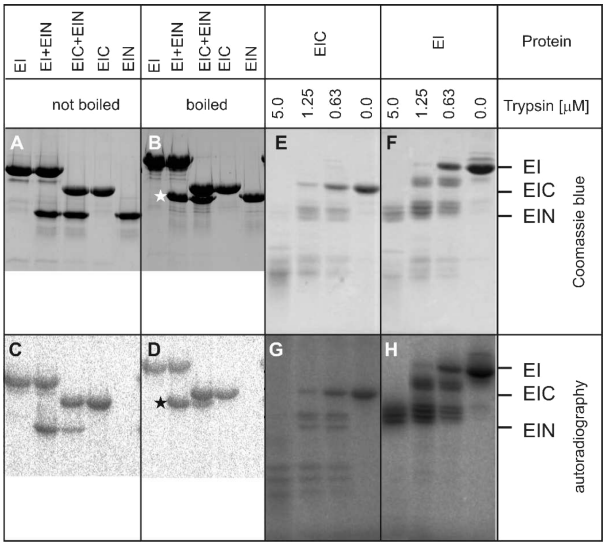


FIGURE 4: Phosphorylation of EI with [$^{32}$P]PEP. (A−D) EI, EIN, and EIC were incubated with [32P]PEP at 65 °C for 10 min. The samples were diluted in SDS sample buffer, boiled or not boiled, and analyzed by SDS−PAGE. The gels were first autoradiographed (C and D) and then stained with Coomassie blue (A and B). The asterisk denotes EIN that completely unfolds only when boiled [100 °C for 3 min (B and D)]. Notice that besides EIN (in the presence of EI or EIC) and full-length EI, the PEP-binding EIC domain also remains radiolabeled after heat denaturation, while EIN without EI or EIC is not phosphorylated (because covalent phosphorylation of EIN and EI at His189 is catalyzed by EIC). (E−H) Partial trypsinolysis of [$^{32}$P]PEP-labeled EIC and EI. Radiolabeled peptides of EIC (G) and of predominantly the EIN domain of EI (H).

at 90 °C (Figure S1B of the Supporting Information). The initial increase in negative ellipticity is thought to reflect a transition from long-range $\beta$-interactions in the folded polypeptide backbone to short-range α interactions of an unfolding intermediate. Similar increases in negative ellipticity have been observed with EIIA$^{Glc}$ from *Mycoplasma capricolum* (*24*) and with other $\beta$-sheet proteins (*25*, *26*).

EI is a homodimer of subunits, which consist of two independently folding domains, the monomeric, HPr-binding EIN domain (28 kDa) and the dimeric, PEP-binding EIC domain (35 kDa) (*27*−*29*). The unfolding transition of EI is less cooperative than those of the other PTS proteins (Figure S1 of the

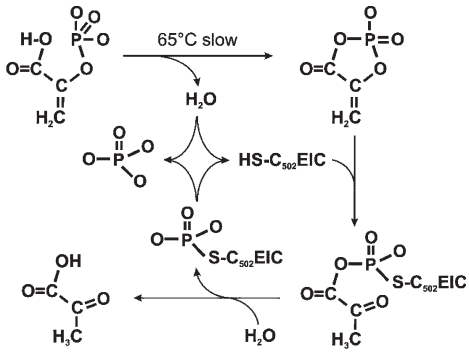


FIGURE 5: Proposed reaction mechanism resulting in a covalent bond between EIC and PEP. Elimination of water affords a cyclic anhydride, which reacts with a nearby nucleophile (e.g., Cys502) to form the putative covalent EIC−PEP adduct. The latter is slowly hydrolyzed, resulting in the formation of pyruvate and inorganic phosphate.

Supporting Information), and its steepness and location vary in the absence and presence of PEP (Figure S2A,E of the Supporting Information). Unphosphorylated EI shows two overlapping transitions at 90 and 95 °C. Upon phosphorylation with PEP, EI shows only one transition at 91 °C (Figure 5A,E). As detailed in the Supporting Information, PEP has no or minimal influence on the thermal stability of EIC, while the stability of EIN is measurably decreased upon phosphorylation at His189, as described previously for the amino-terminal domain of *E. coli* enzyme I (*30*). Such a destabilization increases the potential for unidirectional phosphoryl transfer from EIN to the phosphoryl carrier protein HPr.

*Protein Phosphorylation of EI and EIICB$^{GlcNAc}$.* Two PTS proteins, EIICB$^{GlcNAc}$ and EI, in their phosphorylated states had unexpected properties. Phospho-EIICB$^{GlcNAc}$ was unusually stable and exhibited a strong electrophoretic mobility shift (Figure 2). The EIC domain of EI formed a covalent adduct with PEP.

EIICB$^{GlcNAc}$, by analogy with *E. coli* EIICB$^{Glc}$, is phosphorylated at Cys416 of the B-domain (*31*). Phosphothioester bonds usually are labile, but a significant proportion of EIICB$^{GlcNAc}$ remained phosphorylated through all steps of EIICB$^{GlcNAc}$ expression at 37 °C and purification at 4 °C. To estimate the half-life ($t_{1/2}$) of the hydrolysis resistant phosphothioester, EIICB$^{GlcNAc}$

was phosphorylated at 65 °C with PEP in the presence of catalytic amounts of EI, HPr, and $EIIA^{GlcNAc}$. After the removal of excess PEP by incubation with Prv kinase and ADP at 37 °C, the mixture was kept at room temperature and samples were taken periodically for analysis by SDS−PAGE (Figure S3A,B of the Supporting Information). The half-life of phospho-$EIICB^{GlcNAc}$ estimated by densitometry of the Coomassie-stained protein bands was 4 h for the wild type and 60 h for the K113E/R411K/R413K mutant (Figure S3C of the Supporting Information). The latter lacks the two invariant arginines essential for the forward transfer of phosphate from the EIIB domain to Glc (*32*), and in the absence of Glc to water. Notice that the mutant $EIICB^{GlcNAc}$ after extensive purification was still 50% phosphorylated while the wild type was dephosphorylated (compare the leftmost lanes of Figure S3A,B of the Supporting Information).

EI by analogy with *E. coli* EI is phosphorylated at His189 of the EIN domain. This phosphohistidine bond is rather stable, too, as suggested by the bimodal thermal unfolding behavior of purified EI (see Figure S2A of the Supporting Information). Wild-type *T. tengcongensis* EI was autophosphorylated (*cis* phosphorylation) and competent to *trans* phosphorylate an isolated EIN domain (Figure 4C,D, lanes 1 and 2), which has been described for EI of *E. coli* (*33*). Similarly, the isolated EIC domain was competent to (*trans*) phosphorylate an isolated EIN domain (Figure 4C,D, lane 3). Unexpectedly, ~20% of the total EIC was also radiolabeled in this reaction (Figure 4C,D, lanes 3 and 4), while EIN alone was not (Figure 4C,D, lane 5). Whereas the EIN domain and full-length EI are known to be covalently labeled at His189, the EIC domain was expected to bind [$^{32}$P]PEP noncovalently and to therefore lose it in the presence of SDS. However, the radiolabeled EIC was resistant to boiling in SDS, suggesting a covalent bond. The notion of covalent labeling was confirmed by limited proteolysis of EI and EIC, which both produced a series of radiolabeled peptides (Figure 4E,G). A similar pattern of radiolabeled peptides was also obtained with chymotrypsin (results not shown). The shortest of all, a chymotryptic peptide from EIC, was identified by Edman sequencing to start with residue 460 (results not shown). This locates the radioactive moiety at one (or several) of the most C-terminal 100 residues of EIC. Electrospray ionization mass spectrometry of PEP-treated EIC indicated a molecular mass of 38315.00 Da that is equal to the mass of the EIC polypeptide (38165 Da) plus 150 Da. The latter corresponds to PEP (168 Da) minus water (18 Da), suggesting that PEP condensed with EIC. Further attempts to identify the modified amino acid residue by mass spectrometry were unsuccessful. [$^{32}$P]PEP labeling of active site mutants of full-length EI(H189A), EI(C502A), and the EIC(C502A) domain revealed the following (Figure S4 of the Supporting Information): Only the isolated EIC domain was radiolabeled, not EI(H189A), although this full-length protein contains an unaltered, fully functional EIC domain. EI(C502A) was weakly labeled, suggesting that His189 is phosphorylated slowly by EIC even in the absence of the invariant Cys502. In contrast, EIC(C502A) is not labeled.

We speculate that the covalent adduct is a major side product, which forms during incubation of EIC with PEP at 65 °C. No such product is obtained at room temperature where only the noncovalent PEP−EIC complex is formed (see below). The covalent adduct may be formed as follows (*34*): A cyclic phosphate enol ester/phosphate carboxylate mixed anhydride of PEP is formed by the elimination of water at elevated temperatures (Figure 5). Water elimination may be favored by the apolar milieu of the PEP binding site. An electrophilic center ($C_1$ of PEP or P) of the cyclic intermediate then reacts with a nearby nucleophile, most likely Cys502. This residue indeed is in the covalently labeled peptide (residues 460−573), and the C502A mutant is not labeled. Water elimination is a slow side reaction, which occurs only when the phosphate cannot be rapidly transferred to His189. Moreover, the EIN domain, even an inactive H189A one, if present in *cis* (on the same EI subunit), appears to slow or prevent the formation of the cyclic phosphate.

The PEP−-EIC adduct that formed at 65 °C was crystallized at room temperature with the objective of elucidating its covalent structure. However, instead of a ligand expected to be covalently bound to EIC, only a molecule of Prv could be detected in the active site (see below). This Prv could have been formed from the metastable covalent EIC−PEP intermediate during the 3 week crystallization. A possible reaction mechanism is depicted in Figure 5.

*X-ray Structures of the EIC−PEP and EIC−Prv Complexes*. EI of the PTS consists of two domains, the N-terminal EIN domain and the C-terminal EIC domain. EIC contains the PEP binding site. EIN consists of two subdomains, the histidine domain and the binding domain for the phosphoryl carrier protein HPr. Models of full-length phosphorylated and nonphosphorylated EI monomers with the EIC domain colored green are shown in Figure 7B. The phosphorylated form of full-length *E. coli* EI (*Ec*EI) and the apo form of full-length *S. aureus* EI (*Sa*EI) have been described previously (*27*, *28*). The EIC domain features an $(\beta\alpha)_8$ barrel with three large helical insertions between $\beta2$ and $\alpha2$, $\beta3$ and $\alpha3$, and $\beta6$ and $\alpha6$, which protrude approximately 30 Å above the core of the barrel. The active site Cys502 (*33*) is located in the $\beta7-\alpha7$ turn. EIC is a dimer with an amphipathic dimer interface with an area of 3750 Å$^2$ per monomer.

Models of the *T. tengcongensis* EIC monomer domain (*Tt*EIC), with a molecule of PEP and Prv in the active site, are shown in Figure 6. Refinement of the native protein structures against 1.83 and 1.68 Å data resulted in *R* factors of 16.5 and 17.4% and $R_{free}$ values of 19.4 and 19.7%, respectively, with good stereochemistry (Table 1).

Crystallization of the *Tt*EIC domain that had been preincubated with PEP for 10 min at 65 °C (as described above) afforded the EIC−Prv complex. Cocrystallization of *Tt*EIC and PEP at room temperature afforded the EIC−PEP complex. The comparison of the EIC−PEP and EIC−Prv complexes with the *Tt*EIC apo form [Protein Data Bank (PDB) entry 2WQD] shows only minor deviations for the paired $C_\alpha$ chains (rmsd of 0.33 Å). Substantial structural changes relative to the apo form occur, however, in the side chain conformations of the active site upon binding of PEP (to be described below). Binding of Prv, in contrast, has almost no effect (Figure 6B,C).

PEP binding is achieved by a set of conserved residues as follows (Figures 6B,C and 7C,D). The phosphate moiety of PEP is coordinated by three arginines (R296, R332, and R465), ND2 of Asn454, and $Mg^{2+}$. The carboxyl group of PEP is coordinated by $Mg^{2+}$ and the backbone amides of Asn454 and Asp455. The $Mg^{2+}$ is surrounded by seven ligands in a distorted pentagonal bipyramidal geometry as follows: axially by the phosphate oxygen of PEP and the carboxyl oxygen of Glu431 and equatorially by the carboxylate oxygen of PEP, the carboxylate of Asp455, and three water molecules (Figure 7C,D). Prv is coordinated by the same residues as PEP, its keto group by the guanidino group of Arg332 and $Mg^{2+}$, and its carboxyl group by backbone nitrogens of Asn454 and Asp455. With a water molecule instead of the

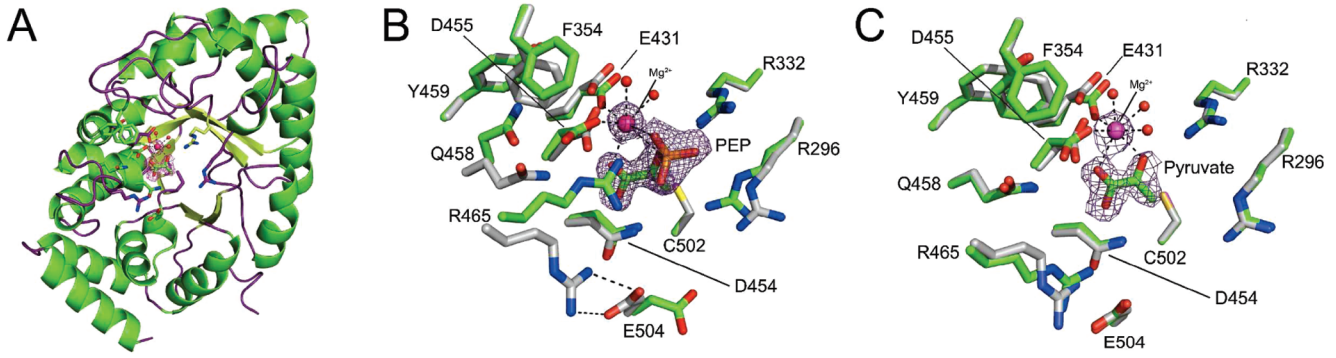


FIGURE 6: Structure of the *T. tengcongensis* EIC domain in complex with PEP and pyruvate. (A) Cartoon model of the pyruvate form seen from the top of the $\beta\alpha$ barrel. Only one subunit of the homodimer is shown. (B) Stick representation of the PEP binding (green) and the apo (gray) states represented in the same orientation as in panel A. (C) Stick representation of the pyruvate binding (green) and the apo (gray) states, represented in the same orientation as in panel A. The side chain conformations of the PEP binding state differ significantly from the apo state, while those of the pyruvate state are almost identical with those of the apo state (compare B and C). The arrows in panel B indicate the main rearrangements between the two binding states. Notice the two conformations of the Phe354 (F354) ring in the pyruvate form (C), one stacking with Tyr459 (Y459) as in the apo state and the other nonstacking as in the PEP state. The $2F_o - F_c$ composite annealed omit electron density maps of PEP and pyruvate are depicted in chicken wire representation and contoured 2.0 (PEP) and 1.4 (Prv) standard deviations above the mean. Atomic colors are as follows: oxygen, red; nitrogen, blue; sulfur, yellow; carbon, green and gray; phosphorus, gold; magnesium, magenta; water, red spheres.

phosphate oxygen of PEP as a ligand, the coordination sphere of $Mg^{2+}$ becomes even more distorted. The two pyruvate molecules in the asymmetric unit were refined to occupancies of 83 and 70%, respectively. The small difference is due to the fact that the electron density of the B chain pyruvate is slightly less well-defined than of the A chain pyruvate.

Binding of PEP causes substantial changes in the side chain conformations of the *Tt*EIC active site, as depicted in panels B and C of Figure 6. The comparison of these local changes between the *Tt*EIC−PEP and *Tt*EIC−Prv complexes on one hand with the global changes in the domain conformation between the phospho-*Ec*EI−oxalate complex (PDB entry 2HWG) and apo *Sa*EI (PDB entry 2WQD) on the other (Figure 7B) suggests a mechanism by which the binding of PEP and domain interactions and/or movements are coupled. The domain movements are shown in Figure 7B. Panels C and D of Figure 7 show the local changes in the PEP binding site of the EIC domain and at the interface between EIC and the histidine subdomain (yellow), to which the phosphate is transferred. The transition from the PEP-bound to the Prv-bound (or apo) state causes the following conformational changes in the EIC active site (Figure 7C,D). Arg465 is shifted by 4.8 Å out of the active site to form a new salt bridge with the carboxylate of Glu504 instead of the phosphate moiety of PEP. Formation of this alternative salt bridge drags the side chain of Glu504 from its surface-exposed position toward the active site. The functional consequence of this rearrangement for the domain interaction will be discussed below. The switch from the Arg465−PEP to the Arg465−Glu504 salt bridge entails further rearrangements. (i) The Arg465 main chain is shifted in the same direction. (ii) The space generated by the shift of Arg465 is filled by a 2.7 Å movement of Gln458. (iii) The Gln458 shift allows the Phe354 aromatic ring to assume an alternative conformation, namely a 70° rotation to $\pi-\pi$ stack with the nearby Tyr459; 54% of the Phe354 rings are rotated (occupancy refined), and 46% retain the conformation of the PEP form. Finally, Arg296, which is across from Arg465, also is shifted by 1.6 Å out of the active site. Together, the side chain rearrangements that follow the dephosphorylation of PEP open the active site and thus facilitate the release of Prv.

The possible role of Glu504 as a switch can be gleaned from the structural superpositions of the PEP−*Tt*EIC complex and full-length phospho-*Ec*EI on one hand (Figure 7C) and of the apo/Prv forms of *Tt*EIC and full-length *Sa*EI on the other (Figure 7D). The structures of full-length phospho-*Ec*EI in a complex with the enolpyruvate analogue oxalate and of apo *Sa*EI have been described extensively, and it has been shown that the two models (Figure 7B) represent two functionally relevant conformations (*27*, *28*). (i) The phospho-*Ec*EI structure shows a snapshot of the conformation immediately after in-line transfer of phosphate from PEP to His191 on the EIN domain. (ii) In apo *Sa*EI, the EIN domain is rotated away from EIC, and the conformation is appropriate for in-line transfer of the phosphate from His191 to the active site histidine of the phosphoryl carrier protein HPr. Full-length *Sa*EI and *Ec*EI are 54% identical in sequence to *Tt*EI. The EIC domains of *Ec*EI and *Sa*EI are 59% identical to *Tt*EIC. Using COOT (*35*), 305 residues of *Tt*EIC can be superimposed with the EIC domain of full-length *Ec*EI (PDB entry 2HWG) with an rmsd of 1.17 Å for the paired $C_\alpha$ atoms. The superposition with full-length *Sa*EI (PDB entry 2WQD) affords a rmsd of 0.34 Å. Most striking in the *Ec*EI−*Tt*EIC superposition is the perfect overlap of the phosphoryl moieties of PEP from *Tt*EIC and of phospho-His191 from *Ec*EI (Figure 7A). Similarly, the enolpyruvoyl moiety of PEP in *Tt*EIC as well as of the oxalate in *Ec*EI and all the active site residues characterized above are also perfectly aligned. The same holds for the comparison of apo full-length *Sa*EI with the apo/Prv−*Tt*EIC domain, with the exception of *Sa*EI Glu506, which does not assume the same conformation as the equivalent Glu504 of the apo/Prv−*Tt*EIC complex. However, the increase in the *B* factor of Glu506 by more than 15 $Å^2$ compared to the surrounding indicates a high flexibility of this residue.

The model (Figure 7C) of phosphorylated *Ec*EI shows that Glu504 on EIC interacts with Arg186 and Arg195 of EIN maintaining the phosphorylated His189 of EIN close to the PEP binding site of EIC. Arg465 interacts with the phosphate moiety of PEP (as described above, Figure 6B), P∼His189 (Figure 7C), and probably also the transition state between PEP and His189. Upon completion of the phosphoryl transfer, Arg465 moves away to form a new salt bridge with Glu504 (Figure 7D). In other words, the Glu504−Arg186/Arg195 salt bridge stabilizes the EIN domain in a conformation appropriate for in-line transfer of the phosphoryl moiety from PEP to His191. The Arg465−phosphate

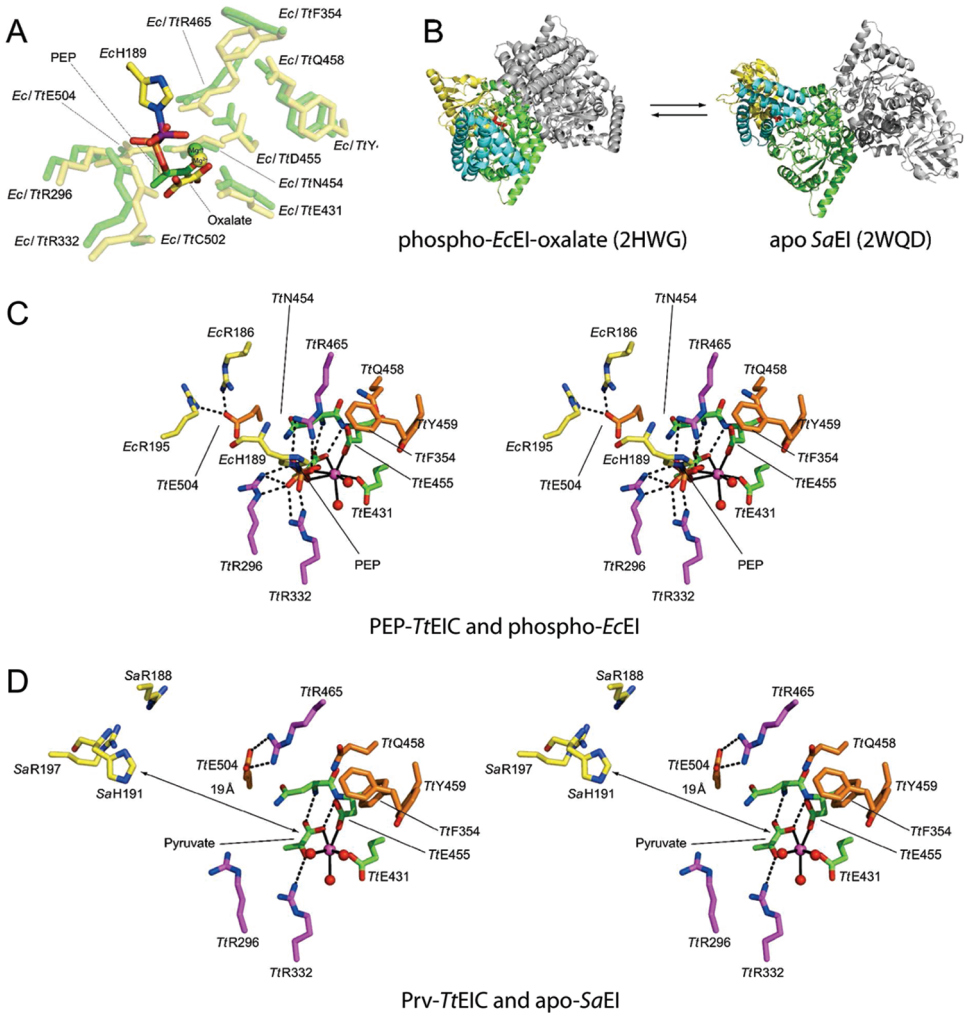


FIGURE 7: Switching function of Glu504 (E504). (A) Stick representation of the overlay between the PEP−*Tt*EIC complex (green, Figure 6A) and the full-length phospho-*Ec*EI−oxalate complex [yellow, PDB entry 2HWG (*28*)]. Notice the perfect overlay of the phosphoryl groups of PEP (*Tt*) and phospho-His189 (*Ec*H189). (B) Cartoon models of the full-length phospho-*Ec*EI−oxalate complex (PDB entry 2HWG) and apo *Sa*EI (PDB entry 2WQD). The PEP binding EIC domains are colored green, the histidine subdomains of EIN yellow, and the HPr-binding subdomains of EIN cyan. The second subunits of the homodimers are colored gray. (C) Stereoview of the EIC domain active site geometry of the PEP-bound *Tt*EIC domain and relevant residues (yellow) of the *Ec*EI histidine subdomain in the phosphorylated state. (D) Stereoview of the EIC domain active site geometry of the pyruvate-bound *Tt*EIC domain and the relevant residues (yellow) of the *Sa*EI apo state. The ligands forming the first ligand shell around the phosphoryl moiety are colored purple and those around the carboxylate and $Mg^{2+}$ green. The residues of the second ligand shell are colored orange. The residues of the EIN histidine subdomain are always colored yellow. The alternative salt bridges between Glu504 (*Tt*E504) and Arg186/Arg195 (*Ec*R186/*Ec*R195) (C) and between Glu504 (*Tt*E504) and Arg465 (*Tt*R465) (D) and all other hydrogen and salt bridges are shown as dashed lines; $Mg^{2+}$ (magenta) coordination is shown as solid lines. Notice that Phe354 (*Tt*F354) occurs in two approximately equally populated conformations in the Prv form (D). Orientation of panels C and D relative to panel B: panel B rotated −35° around the vertical and 90° around the horizontal axes in the plane of the picture with the $Mg^{2+}$ as the center of rotation. For details, see the text.

interaction stabilizes the phosphoryl group in the transition state. After phosphate transfer, Arg465 forms an alternative salt bridge with the carboxylate of Glu504. The Glu504−Arg186/Arg195 salt bridge is broken, and as a consequence, the now phosphorylated EIN domain is released and can swing away from the EIC domain by 19 Å (Figure 7D) to hand on the phosphoryl group to the phosphoryl carrier protein HPr.

*Conclusion*. Thermophilic *T. tengcongensis* and mesophilic *E. coli* PTS proteins share between 60 and 30% sequence identity. Membrane and soluble proteins of the *T. tengcongensis* PTS were purified and characterized with the objective of obtaining thermostable orthologues of the *E. coli* PTS for crystallization experiments. Soluble *T. tengcongensis* proteins could be expressed with good yields in *E. coli*. Of the membrane transporters, only two could be expressed in satisfactory amounts and quality. Of the others, $EIIC^{Gat}$ was produced in overly small amounts, and $EIICD^{Man}$ and $EIIC^{Chb}$ were not expressed at all. The open reading frame for $EIIC^{Mtl}$ could not be cloned, most likely because this membrane protein, or a stable fragment thereof, is toxic. High-throughput crystallization screens with membrane proteins $EIICB^{GlcNAc}$ and $EIIBC^{Fru}$ and the $EIIC^{Fru}$ domain alone and in complex with Fab fragments were promising, but the crystals did not diffract and were inferior to those obtained with the EIIC domain of *E. coli* $EIICB^{Glc}$ (*36*). The *T. tengcongensis* proteins are resistant to thermal unfolding with $T_m$ values between 85 and 95 °C, and their phosphorylated forms are also much more resistant to hydrolysis of the phosphohistidine and phosphocysteine bonds. The X-ray structures of the EIC−PEP and EIC−Prv complexes provide a plausible picture of how the substrate and the product are bound and how transfer of a phosphoryl group from PEP to His189 of EI may trigger the side chain rearrangement that

ultimately results in undocking of the phosphorylated EIN domain from EIC. A potentially interesting side reaction is the formation of a metastable covalent adduct between PEP and the PEP-binding C-terminal domain of EI. We speculate that a cyclic phosphate intermediate of PEP is formed in the active site, which then reacts with the thiol group of nearby Cys502. Although the covalent adduct that can be detected via SDS−PAGE accounts for only 20% of total EIC, this side reaction reveals a mechanism for EI suicide inhibition that may be further developed in the future (*37*−*39*).

## ACKNOWLEDGMENT

We thank Karin Flückiger-Brühwiler for technical support.

## SUPPORTING INFORMATION AVAILABLE

Details on cloning, expression, and protein purification; thermal unfolding and circular dichroism spectroscopy; and phosphotransferase activity and protein phosphorylation assays. This material is available free of charge via the Internet at http://pubs.acs.org.

## REFERENCES

1. Kundig, W., Gosh, S., and Roseman, S. (1964) Phosphate bound to histidine in protein as an intermediate in a novel phosphotransferase system. *Proc. Natl. Acad. Sci. U.S.A. 52*, 1067–1074.
2. Deutscher, J., Francke, C., and Postma, P. W. (2006) How phosphotransferase system-related protein phosphorylation regulates carbohydrate metabolism in bacteria. *Microbiol. Mol. Biol. Rev. 70*, 939–1031.
3. Hogema, B. M., Arents, J. C., Inada, T., Aiba, H., Van Dam, K., and Postma, P. W. (1997) Catabolite repression by glucose 6-phosphate, gluconate and lactose in *Escherichia coli*. *Mol. Microbiol. 24*, 857–867.
4. Takahashi, H., Inada, T., Postma, P., and Aiba, H. (1998) CRP down-regulates adenylate cyclase activity by reducing the level of phosphorylated IIA(Glc), the glucose-specific phosphotransferase protein, in *Escherichia coli*. *Mol. Gen. Genet. 259*, 317–326.
5. Barabote, R. D., and Saier, M. H., Jr. (2005) Comparative genomic analyses of the bacterial phosphotransferase system. *Microbiol. Mol. Biol. Rev. 69*, 608–634.
6. Saier, M. H., Hvorup, R. N., and Barabote, R. D. (2005) Evolution of the bacterial phosphotransferase system: From carriers and enzymes to group translocators. *Biochem. Soc. Trans. 33*, 220–224.
7. Bolhuis, H. H., Palm, P. P., Wende, A. A., Falb, M. M., Rampp, M. M., Rodriguez-Valera, F. F., Pfeiffer, F. F., and Oesterhelt, D. D. (2006) The genome of the square archaeon *Haloquadratum walsbyi*: Life at the limits of water activity. *BMC Genomics 7*, 169.
8. Peterkofsky, A., Wang, G., Garrett, D. S., Lee, B. R., Seok, Y. J., and Clore, G. M. (2001) Three-dimensional structures of protein-protein complexes in the *E. coli* PTS. *J. Mol. Microbiol. Biotechnol. 3*, 347–354.
9. Daley, D. O., Rapp, M., Granseth, E., Melen, K., Drew, D., and von Heijne, G. (2005) Global Topology Analysis of the *Escherichia coli* Inner Membrane. *Proteome Sci. 308*, 1321–1323.
10. Vervoort, E. B., Bultema, J. B., Schuurman-Wolters, G. K., Geertsma, E. R., Broos, J., and Poolman, B. (2005) The first cytoplasmic loop of the mannitol permease from *Escherichia coli* is accessible for sulfhydryl reagents from the periplasmic side of the membrane. *J. Mol. Biol. 346*, 733–743.
11. Huber, F., and Erni, B. (1996) Membrane topology of the mannose transporter of *Escherichia coli* K12. *Eur. J. Biochem. 239*, 810–817.
12. Reizer, J., Mitchell, W. J., Minton, N., Brehm, J., Reizer, A., and Saier, M. H. (1996) Proposed topology of the glucitol permeases of *Escherichia coli* and *Clostridium acetobutylicum*. *Curr. Microbiol. 33*, 331–333.
13. Buhr, A., and Erni, B. (1993) Membrane topology of the glucose transporter of *Escherichia coli*. *J. Biol. Chem. 268*, 11599–11603.
14. Jacobson, G. R., Kelly, D. M., and Findley, D. R. (1983) The intramembrane topography of the mannitol-specific Enzyme II of the *Escherichia coli* phosphotransferase system. *J. Biol. Chem. 258*, 2955–2959.
15. Bao, Q., Tian, Y., Li, W., Xu, Z., Xuan, Z., Hu, S., Dong, W., Yang, J., Chen, Y., Xue, Y., Xu, Y., Lai, X., Huang, L., Dong, X., Ma, Y., Ling, L., Tan, H., Chen, R., Wang, J., Yu, J., and Yang, H. (2002) A complete sequence of the *T. tengcongensis* genome. *Genome Res. 12*, 689–700.
16. Kundig, W., and Roseman, S. (1971) Sugar transport. II. Characterization of constitutive membrane-bound enzymes II of the *Escherichia coli* phosphotransferase system. *J. Biol. Chem. 246*, 1407–1418.
17. Erni, B., Trachsel, H., Postma, P. W., and Rosenbusch, J. P. (1982) Bacterial phosphotransferase system. Solubilization and purification of the glucose-specific enzyme II from membranes of *Salmonella typhimurium*. *J. Biol. Chem. 257*, 13726–13730.
18. Erni, B. (1986) The glucose-specific permease of the bacterial phosphotransferase system: Phosphorylation and oligomeric structure of the glucose-specific IIGlc/IIIGlc complex of *Salmonella typhimurium*. *Biochemistry 25*, 305–312.
19. Claros, M. G., and von Heijne, G. (1994) TopPred II: An improved software for membrane protein structure predictions. *Comput. Appl. Biosci. 10*, 685–686.
20. Juretic, D., Zoranic, L., and Zucic, D. (2002) Basic charge clusters and predictions of membrane protein topology. *J. Chem. Inf. Comput. Sci. 42*, 620–632.
21. Tian, L. (2009) Biochemical characterization and preliminary X-ray analysis of mannose transporter complexes from *Escherichia coli*. Ph.D. Thesis, University of Bern, Bern, Switzerland.
22. Decurtins, C. (2005) Production of carbohydrate transport proteins and conformation-sepcific antibodies for co-crystallization. Diploma Thesis, University of Bern, Bern, Switzerland.
23. Bao, Q., Tian, Y., Li, W., Xu, Z., Xuan, Z., Hu, S., Dong, W., Yang, J., Chen, Y., Xue, Y., Xu, Y., Lai, X., Huang, L., Dong, X., Ma, Y., Ling, L., Tan, H., Chen, R., Wang, J., Yu, J., and Yang, H. (2002) A complete sequence of the *T. tengcongensis* genome. *Genome Res. 12*, 689–700.
24. Zhu, P. P., Nosworthy, N., Ginsburg, A., Miyata, M., Seok, Y. J., and Peterkofsky, A. (1997) Expression, purification, and characterization of enzyme $IIA^{glc}$ of the phosphoenolpyruvate:sugar phosphotransferase system of *Mycoplasma capricolum*. *Biochemistry 36*, 6947–6953.
25. Jayaraman, G., Kumar, T. K., Sivaraman, T., Lin, W. Y., Chang, D. K., and Yu, C. (1996) Thermal denaturation of an all $\beta$-sheet protein: Identification of a stable partially structured intermediate at high temperature. *Int. J. Biol. Macromol. 18*, 303–306.
26. Narhi, L. O., Philo, J. S., Li, T., Zhang, M., Samal, B., and Arakawa, T. (1996) Induction of $\alpha$-helix in the $\beta$-sheet protein tumor necrosis factor-$\alpha$: Thermal- and trifluoroethanol-induced denaturation at neutral pH. *Biochemistry 35*, 11447–11453.
27. Oberholzer, A. E., Schneider, P., Siebold, C., Baumann, U., and Erni, B. (2009) Crystal structure of enzyme I of the phosphoenolpyruvate: sugar phosphotransferase system in the dephosphorylated state. *J. Biol. Chem. 284*, 33169–33176.
28. Teplyakov, A., Lim, K., Zhu, P. P., Kapadia, G., Chen, C. C., Schwartz, J., Howard, A., Reddy, P. T., Peterkofsky, A., and Herzberg, O. (2006) Structure of phosphorylated enzyme I, the phosphoenolpyruvate: sugar phosphotransferase system sugar translocation signal protein. *Proc. Natl. Acad. Sci. U.S.A. 103*, 16218–16223.
29. Garrett, D. S., Seok, Y. J., Peterkofsky, A., Gronenborn, A. M., and Clore, G. M. (1999) Solution structure of the 40,000 Mr phosphoryl transfer complex between the N-terminal domain of enzyme I and HPr. *Nat. Struct. Biol. 6*, 166–173.
30. Nosworthy, N. J., Peterkofsky, A., Konig, S., Seok, Y. J., Szczepanowski, R. H., and Ginsburg, A. (1998) Phosphorylation destabilizes the amino-terminal domain of enzyme I of the *Escherichia coli* phosphoenolpyruvate:sugar phosphotransferase system. *Biochemistry 37*, 6718–6726.
31. Meins, M., Jeno, P., Muller, D., Richter, W. J., Rosenbusch, J. P., and Erni, B. (1993) Cysteine phosphorylation of the glucose transporter of *Escherichia coli*. *J. Biol. Chem. 268*, 11604–11609.
32. Lanz, R., and Erni, B. (1998) The glucose transporter of the *Escherichia coli* phosphotransferase system: Mutant analysis of the invariant arginines, histidines, and domain linker. *J. Biol. Chem. 273*, 12239–12243.
33. Garcia-Alles, L. F., Flükiger, K., Hewel, J., Gutknecht, R., Siebold, C., Schürch, S., and Erni, B. (2002) Mechanism-based inhibition of enzyme I of the *Escherichia coli* phosphotransferase system: Cysteine 502 is an essential residue. *J. Biol. Chem. 277*, 6934–6942.
34. O'Neal, C. C., Jr., Bild, G. S., and Smith, L. T. (1983) Facile oxygen exchanges of phosphoenolpyruvate and preparation of [$^{18}$O]phosphoenolpyruvate. *Biochemistry 22*, 611–617.
35. Emsley, P., and Cowtan, K. (2004) Coot: Model-building tools for molecular graphics. *Acta Crystallogr. D60*, 2126–2132.

36. Zurbriggen, A., Schneider, P., Bahler, P., Baumann, U., and Erni, B. (2010) Expression, purification, crystallization and preliminary X-ray analysis of the EIICGlc domain of the *Escherichia coli* glucose transporter. *Acta Crystallogr. F66*, 684–688.
37. Kok, M., Bron, G., Erni, B., and Mukhija, S. (2003) Effect of enzyme I of the bacterial phosphoenolpyruvate:sugar phosphotransferase system (PTS) on virulence in a murine model. *Microbiology 149*, 2645–2652.
38. Mukhija, S., Germeroth, L., Schneider-Mergener, J., and Erni, B. (1998) Identification of peptides inhibiting enzyme I of the bacterial phosphotransferase system using combinatorial cellulose-bound peptide libraries. *Eur. J. Biochem. 254*, 433–438.
39. Mukhija, S., and Erni, B. (1997) Phage display selection of peptides against enzyme I of the phosphoenolpyruvate sugar phosphotransferase system (PTS). *Mol. Microbiol. 25*, 1159–1166.
40. Bachler, C., Flukiger-Bruhwiler, K., Schneider, P., Bahler, P., and Erni, B. (2005) From ATP as substrate to ADP as coenzyme: Functional evolution of the nucleotide binding subunit of dihydroxyacetone kinases. *J. Biol. Chem. 280*, 18321–18325.
41. Erni, B., Siebold, C., Christen, S., Srinivas, A., Oberholzer, A., and Baumann, U. (2006) Small substrate, big surprise: Fold, function and phylogeny of dihydroxyacetone kinases. *Cell. Mol. Life Sci. 63*, 890–900.